Bone Healing Response to Different Concentrations of Nano-Hydroxyapatite Incorporated into Mineral Trioxide Aggregate and Bioceramic Sealers

Arkhawan Ali Abdulhaq , Chenar Anwar Mohammad , Bassam Karem Amin *

Posted Date: 18 May 2026

doi: 10.20944/preprints202605.1131.v1

Keywords: nano-hydroxyapatite; bone regeneration; histomorphometry; biomaterials; calcium silicate cement; rabbit model

 doi:10.20944/preprints202605.1131.v1

Article

Bone Healing Response to Different Concentrations of Nano-Hydroxyapatite Incorporated into Mineral Trioxide Aggregate and Bioceramic Sealers

Arkhawan Ali Abdulhaq, Chenar Anwar Mohammad and Bassam Karem Amin *

College of Dentistry, Hawler Medical University, Kurdistan Region, Iraq

* Correspondence: bassam.amin@hmu.edu.krd; Tel.: +9647504459392

Abstract

Nano-engineering strategies have been increasingly applied to enhance the biological performance of calcium silicate–based materials; however, the optimal concentration of nano-hydroxyapatite (HANP) remains unclear. This study evaluated the bone-healing response to different concentrations of HANP incorporated into mineral trioxide aggregate (MTA) and bioceramic (BC) sealers in an experimental rabbit model. Thirty adult New Zealand white rabbits were allocated into two experimental groups according to sealer type: HANP-modified MTA and HANP-modified BC (n = 15 each). Two standardized circular intrabony defects were created bilaterally in the maxillary diastema of each rabbit. In the MTA group, the right-side defects were filled with 2% and 4% HANP-modified MTA, while on the left side one defect received 6% HANP-modified MTA and the adjacent defect was left as control. The same protocol was followed for the BC group using corresponding HANP concentrations. Five rabbits per group were sacrificed at 2, 4, and 8 weeks postoperatively for histopathological hematoxylin and eosin (H&E) and Masson trichrome staining. The results demonstrated significant differences among groups at all-time points, with 4% HANP showing the most favorable biological response, including reduced inflammatory cell infiltration, increased new bone formation, and improved collagen organization compared with lower and higher concentrations. Pairwise comparisons at matched HANP concentrations revealed no statistically significant differences between HANP-modified MTA and BC groups. These findings indicate that HANP incorporation enhances the biological performance of calcium silicate–based sealers in a concentration-dependent manner, with 4% representing an optimal formulation for promoting bone regeneration.

Keywords: nano-hydroxyapatite; bone regeneration; histomorphometry; biomaterials; calcium silicate cement; rabbit model

1. Introduction

A bone defect is characterized by the absence of bone tissue in a particular body component that may develop as a result of trauma, infection, inflammation, injury, or congenital conditions[1]. In certain instances, it may also result from persistent medical conditions or surgical operations [2]. To promote bone regeneration, materials must frequently be surgically implanted [3,4]. In recent decades, autograft materials have largely been used for bone repair because of their superior osteogenesis, inducibility, and bone conduction [5]. In clinical practice, autologous bone grafts remain the preferred treatment for bone repair [6]. Nevertheless, issues with the harvesting process and the scarcity of donor bone restrict this technique's practical use [7]. Because of this, alternate graft materials and other bone replacements are essential for successful bone restorations [8].

The perfect bone substitute should meet requirements including bioresorbability, osteoinduction, and osteoconductiveness [9]. Additionally, it should be thermally nonconductive and immune rejection-free [10]. Many alloplastic materials have been thoroughly investigated for use as

 doi:10.20944/preprints202605.1131.v1

novel bone substitutes, including hydroxyapatite, tri-calciumphosphate, calcium phosphate cement, calcium sulphate, bone morphogenetic protein, ceramic and ceramic composites [11]. Nano-hydroxyapatite-based biomaterials were able to promote the bone repair process without any signs of inflammation. Since the composition of hydroxyapatite is similar to bone minerals, it was anticipated that HA would provide a suitable surface for cell adhesion [12] and because of the lack of protein, it does not cause allergic and immune reactions [13]. Furthermore, the release of calcium ions from the nanocrystalline HA is faster than in coarser crystals. Thus, bioceramics based on nanosized HA is a material of choice for various biomedical applications because of improved mechanical properties, sinterability, densification, cellular attachment, proliferation, and differentiation [14]. The nanostructure of HA also facilitates the adsorption of proteins and growth factors, further promoting the osteoinduction process where new bone tissue is formed at the implant site[15].

MTA's bioactivity is attributed to its ability to promote tissue mineralization and cell migration and proliferation. Calcium silicate, the main ingredient of MTA, changes into calcium hydroxide when it comes into touch with tissue. Calcium hydroxide then breaks down into calcium and hydroxide ions, continuously releasing them into the environment [16]. Because of its composition, which enables cells to adhere and proliferate quickly on its structure, it can aid in bone healing. With direct bone apposition, there is evidence that MTA encourages a positive reaction in the osseous environment. MTA surfaces promote RunX2 expression, matrix formation, and osteoblast cell attachment—all of which are critical for osteogenesis [17].

The newer generation of bioceramic sealers has been developed to show the potential of lasting bioactivity by the diffusion of molecules during and after their setting, and may modulate the apical tissue environment through either direct contact of these molecules with the apical tissues as in cases of extrusion or indirectly by diffusion from the root canal system. After the removal of bacteria, healing of apical periodontitis requires remodeling of the granulomatous tissue and induction of the proliferation of bone marrow stem cells and osteoblast precursors into mature osteoblasts, leading to remineralization of the apical tissues [18].

The optimal biological threshold at which nanoparticle incorporation enhances osteogenesis without compromising tissue compatibility remains unclear. Although nano-engineering approaches have shown promise in improving the bioactivity of calcium silicate-based materials, there is a lack of comparable in vivo studies evaluating different nanoparticle concentrations across various sealer matrices. Addressing this gap is essential for translating nanotechnology-based modifications into clinically relevant regenerative outcomes. Therefore, the present study aimed to evaluate the concentration-dependent bone healing response of mineral trioxide aggregate (MTA) and bioceramic (BC) sealers modified with varying concentrations of nano-hydroxyapatite using histological analysis and Masson's trichrome staining, in an experimental rabbit model. The null hypothesis was that varying concentrations of nano-hydroxyapatite would not significantly affect inflammatory response, new bone formation, or collagen deposition, irrespective of sealer type.

2. Materials and Methods

Hydroxyapatite nanoparticles (MERK, GERMANY) were incorporated into mineral trioxide aggregate (MTA) (MTA Cem, NEXOBIO Co., Korea) and a bioceramic sealer (BC) (ONE-FIL bioceramic sealer, MEDICLUS CO., LTD. Korea) at concentrations of 2%, 4%, and 6% (w/w), according to a protocol previously described in an in vitro study [19] .

2.1. Study Design

The study was conducted in accordance with ARRIVE guidelines for preclinical in vivo studies (NC3Rs, UK) and was approved by the Research Ethics Committee of the College of Dentistry, Hawler Medical University, Erbil, Kurdistan Region-Iraq (reference no. HMUD2425057). All procedures adhered to ethical guidelines for the humane treatment of animals, including appropriate housing, medical care, and anesthesia protocols. The study objectives could not be achieved through

 doi:10.20944/preprints202605.1131.v1

non-animal models, and the minimum necessary number of animals was used to ensure statistical validity. The required sample size was determined by performing a power analysis using G*Power software (version 3.1.9.2; Düsseldorf, Germany) for this experimental animal study. The statistical parameters were set at a power of 80% ($1 - \beta = 0.80$) and a significance level of $\alpha = 0.05$, with an estimated effect size (f) of 0.40, with four experimental conditions (2%, 4%, and 6% HANP-modified sealer and control), corresponding to three degrees of freedom. Power analysis indicated a sample size equivalent to 60 bone defects per material group. Under the split-mouth design, each rabbit contributed four standardized intrabony defects; therefore, 15 rabbits were required per material group, resulting in a total of 30 rabbits. Defects were evaluated at 2, 4, and 8 weeks.

2.2. Animal Selection and Housing

A total of 30 adult male New Zealand white rabbits, aged 6–8 months and weighing 1.5–2 kg, were included in this study, in which 120 maxillary bone defects were created. Animals were housed at the Central Animal Care Facility, College of Pharmacy, Hawler Medical University, Erbil. They were acclimatized for one week before surgery and maintained under standardized environmental conditions (temperature: 19–21 °C; humidity: 45% ± 10%; light/dark cycle: 12:12 h), with free access to water and a standard diet ad libitum. Fifteen rabbits (60 defects) were assigned to the HANP-modified MTA group, and fifteen rabbits (60 defects) were assigned to the HANP-modified BC group. In each rabbit, four standardized intrabony defects (3 mm in diameter and 4 mm in depth) were created on the right and left buccal aspects of the maxillary diastema, according to a previously described protocol [20]. A split-mouth design was used in which the two right-sided defects were assigned to receive 2% and 4% HANP-modified MTA, respectively, whereas the first left-sided defect was filled with 6% HANP-modified MTA and the adjacent defect was left untreated as a control. In the BC group, the same protocol was followed, except that 2%, 4%, and 6% HANP were incorporated into BC sealer [21]. Five rabbits from each group were euthanized at 2, 4, and 8 weeks postoperatively, and the maxillae containing the defect sites were harvested for histopathological analysis, as shown in (Figure 1).

2.3. Surgical Protocol

General anesthesia was induced by intramuscular administration of ketamine hydrochloride (20 mg/kg body weight) and xylazine (0.2 mL/kg body weight, 2%) before surgery. In addition, oxytetracycline (20%) was administered intramuscularly at 1 mL/kg body weight one hour before surgery, and postoperative antibiotic prophylaxis was continued at the same dose for 7 days. To prevent corneal drying during anesthesia, tetracycline ophthalmic ointment was applied. Two surgical incisions were made on each buccal aspect of the natural edentulous diastema, located between the central incisors and premolars, to raise a mucoperiosteal flap (Figure 2a–c). Two standardized intrabony defects were created in each diastema using intermittent drilling with a round bur (size #010), followed by a fissure bur (size #010), under copious irrigation, according to a previously described protocol [20]. Experimental materials were inserted into each defect until completely filled. Flaps were repositioned and sutured using absorbable braided polyglycolic acid 6-0 sutures (Yingmed, China). Five rabbits from each group were euthanized by overdose of ketamine hydrochloride at 2, 4, and 8 weeks postoperatively. The right and left maxillary segments containing the defect sites and surrounding bone were harvested for histopathological analysis.

 doi:10.20944/preprints202605.1131.v1

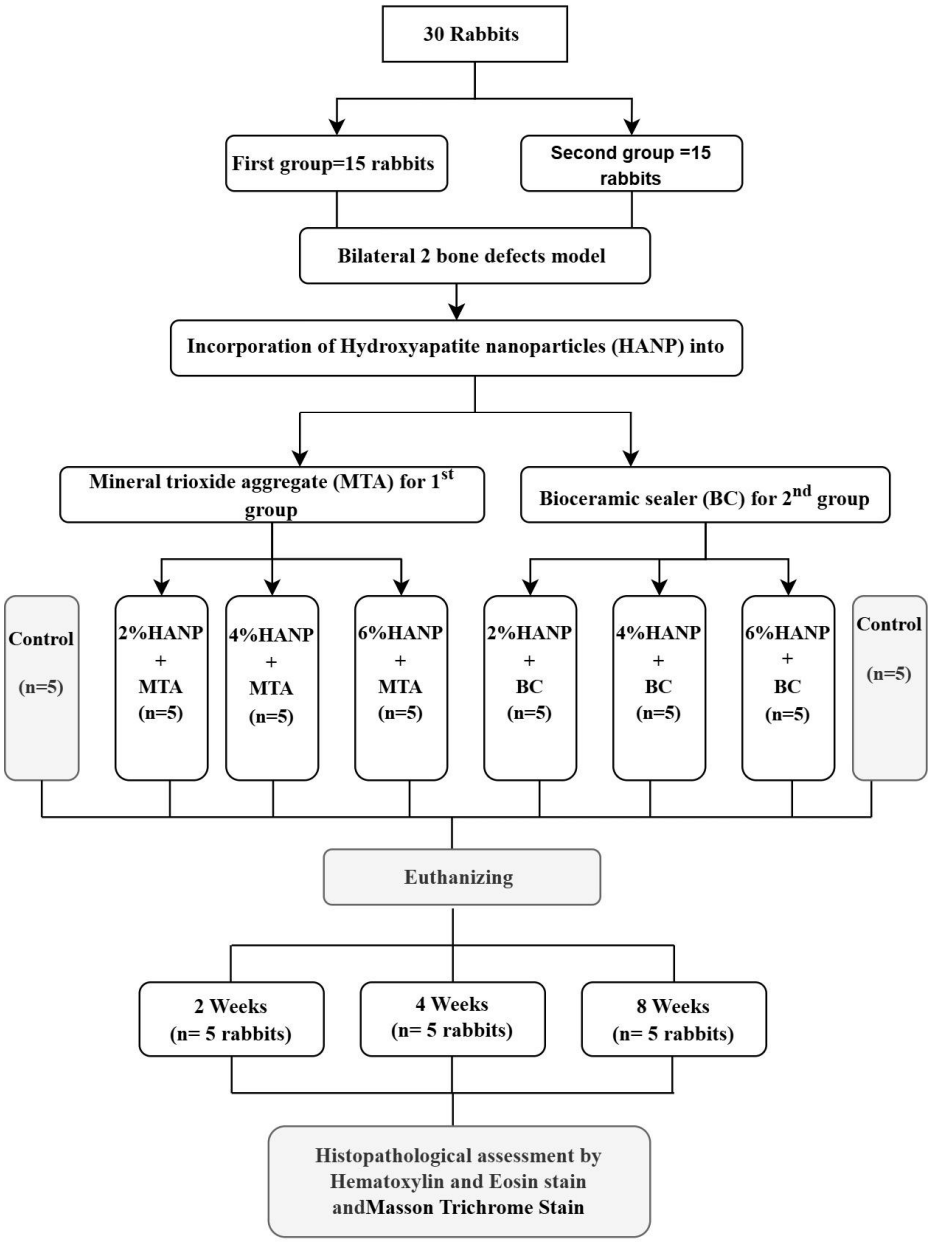

Figure 1. Flowchart showing the experimental stages and their order fulfillment.

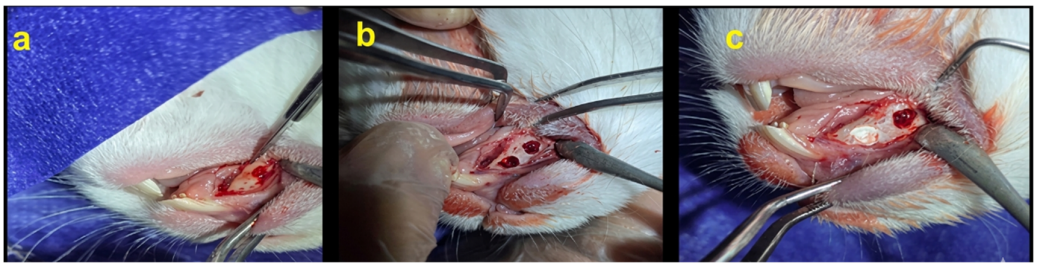

Figure 2. Surgical creation of standardized bone defects in the rabbit maxilla. (a) Exposure of the diastema region following reflection of a full-thickness mucoperiosteal flap. (b) Preparation of the buccal maxillary surface and creation of standardized circular bone defects using a low-speed round bur under continuous sterile saline irrigation. (c) Placement of experimental materials within the defects according to group allocation; control defects were left unfilled.

 doi:10.20944/preprints202605.1131.v1

2.4. Histopathological Assessment

At each predetermined healing interval, defect sites were harvested and fixed by immersion in 10% neutral buffered formalin for 48–72 h, and subsequently decalcified in 10% formic acid for approximately 2–3 days. Following decalcification, the specimens were dehydrated through graded ethanol solutions, cleared in xylene, and embedded in paraffin wax for histological processing. Serial sections approximately 5 μm thick were obtained through the center of each defect using a rotary microtome (Leica RM2135) [22]. Representative photomicrographs were captured and histopathological examination was performed by an experienced histopathologist who was blinded to the experimental groups to reduce observer bias. All slides were assessed at ×40, ×100, and ×400 magnifications [23].

2.5. Histomorphometric Assessment

Quantitative histomorphometric evaluation of bone regeneration within the defect area was performed using a digital light microscope connected to an image analysis system (Motic/ToupTek, ToupView (×86), version 3.7.4183, 2014) at magnifications of ×40, ×100, and ×400. Digital photomicrographs of microscopic fields covering the entire defect region were captured for analysis.

For quantitative analysis, five random microscopic fields per section were evaluated for each animal. All assessments were performed in a blinded manner, and the mean values of the five fields were calculated [24].

The quantity of inflammatory cells was assessed using a semi-quantitative four-point ordinal scale based on the number of inflammatory cells observed per ×400 field as follows: low: no inflammatory cells or extremely few (less than five cells), mild (5 to <25 cells), moderate (25–125 cells), and severe (>125 cells) [25].

New bone formation was assessed using a semi-quantitative histological scoring system. The amount of newly formed bone within the defect area was evaluated under light microscopy and graded as follows: **score 0:** Absence of new bone tissue formation, **score 1:** Discrete—small bone trabeculae covering <25% of the defect area, **score 2:** Moderate—new bone tissue covering ≥50% of the defect area, and **score 3:** Extensive—complete coverage with formation of a bony bridge around the biomaterial tested [26].

2.6. Special Stains

Perl's prussian blue stain was employed to identify iron deposition within the bone trabeculae. The quantity and arrangement of collagen fibers were also evaluated using Goldner's Masson trichrome stain (HistoPlus, Turkey). The following semi-quantitative method was used to assess the degree of collagen organization and maturation [27]: **score 0:** Early, immature collagen fibers organized in a reticular pattern are present. **score 1:** A moderate number of collagen fibers that form weakly cohesive bundles are present. **score 2:** Mature collagen fibers arranged into compact bundles are predominantly present.

2.7. Masson's Trichrome Staining Protocol

After the specimens were fixed and decalcified, paraffin-embedded slices (5 μm) were created. Sections underwent xylene deparaffinization, graded ethanol rehydration, and distilled water washing in preparation for Masson's Trichrome staining. After applying Bouin's solution for one hour at 56 °C to improve staining, the mixture was cooled and rinsed under running water. Biebrich scarlet-acid fuchsin was used for 5 minutes after slices were rinsed and nuclei were stained for 10 minutes with Weigert's iron hematoxylin. Aniline blue was used to stain collagen fibers for five minutes after differentiation was accomplished using phosphomolybdic-phosphotungstic acid solution. This allowed for the evaluation of collagen deposition and new bone development in the defect fields [28,29].

 doi:10.20944/preprints202605.1131.v1

2.8. Statistical Analysis

Statistical analysis was performed using SPSS version 27 (IBM Corp., Armonk, NY, USA). Data were assessed for normality using the Shapiro–Wilk test. As the data were not normally distributed, results were expressed as median and interquartile range (IQR), while mean ± standard deviation (SD) were also reported for descriptive purposes. Intergroup comparisons were performed using the Kruskal–Wallis test, followed by Bonferroni-adjusted post hoc pairwise comparisons. A p-value < 0.05 was considered statistically significant. Graphs were generated using GraphPad Prism version 10 (GraphPad Software Inc., San Diego, CA, USA).

3. Results

3.1. Inflammatory Response

The mean ± standard deviation values, along with median (IQR), of inflammatory response around the implanted materials at 2, 4, and 8 weeks are presented in Table 1. The results demonstrated a higher inflammatory response in the 2% and 6% HANP-containing groups, particularly during the early healing phase (2 weeks), followed by a gradual reduction at later time points. In contrast, defects treated with 4% HANP formulations exhibited the lowest inflammatory response, with a progressive decrease in inflammatory cell infiltration from 2 to 8 weeks in both 4% HANP + MTA and 4% HANP + BC groups.

Table 1. Inflammatory response to different concentrations of hydroxyapatite nanoparticles incorporated into MTA and bioceramic sealers at 2, 4, and 8 weeks.

Group	2 Weeks		4 Weeks		8 Weeks	
	(Mean ± SD)	**(Median [IQR])**	**(Mean ± SD)**	**(Median [IQR])**	**(Mean ± SD)**	**(Median [IQR])**
Control	1.6 ± 0.54^{a}	2 [1–2]	1.4 ± 0.54^{ab}	1 [1–2]	1.4 ± 0.54^{a}	1 [1–2]
2% HANP + MTA	2.2 ± 0.44^{a}	2 [2–2]	2.2 ± 0.44^{a}	2 [2–2]	1.6 ± 0.54^{a}	2 [1–2]
2% HANP + BC	2.2 ± 0.44^{a}	2 [2–2]	1.6 ± 0.89^{a}	1 [1–2]	1.8 ± 0.83^{a}	2 [1–2]
4% HANP + MTA	1.2 ± 0.44^{a}	1 [1–1]	0.6 ± 0.54^{b}	1 [0–1]	0.4 ± 0.54^{a}	0 [0–1]
4% HANP + BC	1.4 ± 0.54^{a}	1 [1–2]	0.6 ± 0.54^{b}	1 [0–1]	0.6 ± 0.54^{a}	1 [0–1]
6% HANP + MTA	2.2 ± 0.44^{a}	2 [2–2]	1.4 ± 0.54^{ab}	1 [1–2]	1.4 ± 0.54^{a}	1 [1–2]
6% HANP + BC	2.0 ± 0.70^{a}	2 [1–2]	1.4 ± 0.89^{ab}	1 [1–1]	1.6 ± 0.54^{a}	2 [1–2]

(SD): standard deviation. Different superscript letters within the same column indicate statistically significant differences among groups ($p < 0.05$); values sharing at least one letter are not significantly different ($p \geq 0.05$).

For pairwise comparison of inflammatory cell response among different groups using Bonferroni-adjusted pairwise comparisons test, (Figure 3), shows that 4% HANP+MTA group at 2 weeks, exhibited significant lower inflammatory scores compared to 6% HANP+BC, 6% HANP+MTA, 2% HANP+MTA, and 2% HANP+BC. Similarly, the 4% HANP+BC group demonstrated significantly reduced inflammatory reaction compared with 6% HANP+MTA, 2% HANP+MTA, and 2% HANP+BC. However, no significant differences were detected between both 4% HANP groups (MTA & BC) at 2 weeks (p= 0.583).

At 4 weeks, 4% HANP groups (MTA & BC) showed significantly lower inflammatory cell response compared to 2% HANP+MTA groups with significant differences were detected between both 4% HANP groups (MTA & BC) at 4 weeks (p=1.000). At 8 weeks. The 4% HANP+MTA group demonstrated significantly reduced inflammatory response compared to control, 6% HANP+BC, 6% HANP+MTA, 2% HANP+MTA, & 2% HANP+BC groups. Likewise, the 4% HANP+BC group showed significantly lower inflammatory scores compared to 6% HANP+BC, 2% HANP+MTA, & 2% HANP+BC group. However, non-significant differences were detected between both 4% HANP groups (p= 0. 712) and among the remaining studied groups comparisons (p > 0.05).

 doi:10.20944/preprints202605.1131.v1

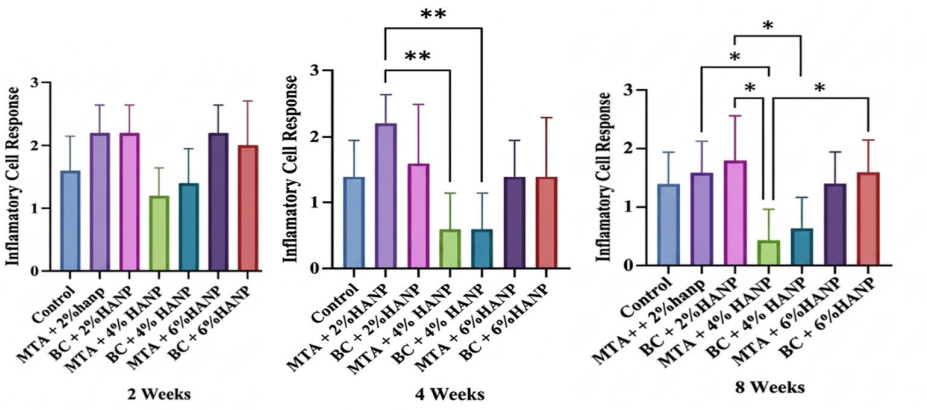

Figure 3. Pairwise comparison for inflammatory cell response of control, MTA and BC sealer-modified with 2%,4% and 6% HANP at 2 Weeks, 4 Weeks and 8 Weeks intervals.

3.2. New Bone Formation

The mean± Standard Deviation, along with median (IQR), of new bone formation around the experimental materials after 2 weeks, 4 weeks and 8 weeks follow up were presented in (Table 2), and shows that The highest new bone formation at all time points was observed in the 4% HANP groups, particularly 4% HANP+MTA, followed by 4% HANP+BC, then the 6% HANP groups, whereas control and 2% HANP+BC exhibited the lowest bone formation.

Table 2. New bone formation scores in control and HANP-modified MTA and BC groups at 2, 4, and 8 weeks.

Group	2 Weeks		4 Weeks		8 Weeks	
	(Mean ± SD)	**(Median [IQR]c)**	**(Mean ± SD)**	**(Median [IQR])**	**(Mean ± SD)**	**(Median [IQR])**
Control	1.2 ± 0.44^{ab}	1 [1–1]	1.0 ± 0.70^{ab}	1 [1–1]	1.4 ± 0.54^{ab}	1 [1–2]
2% HANP + MTA	1.0 ± 0.00^{ab}	1 [1–1]	1.2 ± 0.83^{ab}	1 [1–2]	1.4 ± 0.54^{ab}	1 [1–2]
2% HANP + BC	0.8 ± 0.44^{b}	1 [1–1]	1.0 ± 0.00^{b}	1 [1–1]	1.2 ± 0.44^{b}	1 [1–1]
4% HANP + MTA	2.2 ± 0.44^{a}	2 [2–2]	2.6 ± 0.54^{a}	3 [2–3]	2.6 ± 0.54^{a}	3 [2–3]
4% HANP + BC	2.0 ± 0.70^{ab}	2 [2–2]	2.4 ± 0.54^{ab}	2 [2–3]	2.4 ± 0.54^{ab}	2 [2–3]
6% HANP + MTA	1.6 ± 0.54^{ab}	2 [1–2]	2.0 ± 0.70^{ab}	2 [2–2]	1.8 ± 0.44^{ab}	2 [2–2]
6% HANP + BC	1.4 ± 0.54^{ab}	1 [1–2]	1.4 ± 0.54^{ab}	1 [1–2]	1.6 ± 0.54^{ab}	2 [1–2]

(SD): standard deviation. Different superscript letters within the same column indicate statistically significant differences among groups ($p < 0.05$); values sharing at least one letter are not significantly different ($p \geq 0.05$).

For pairwise comparisons among different studied groups using Bonferroni test, (Figure 4), shows significant variations in new bone formation among different studied groups. At 2 weeks, the 2% HANP+BC group exhibited significantly lower new bone formation compared with 6% HANP+MTA, 4% HANP+BC, and 4% HANP+MTA groups, while 4% HANP+MTA group demonstrated significantly greater bone formation compared to control and 2% HANP+MTA group.

At 4-week, significant higher bone formation was observed in 4% HANP groups (HANP MTA+ BC groups) with non-significant differences between both groups (P= 0.755). Additionally, the 4% HANP+MTA group showed significantly greater bone formation compared to the control, 2% HANP+BC, 2% HANP+MTA, and 6% HANP+BC groups.

At 8 weeks, 4% HANP+MTA &4% HANP+BC groups demonstrated significantly higher bone formation than 2% HANP+BC group, with non-significant differences between both 4% HANP+MTA and 4% HANP+BC groups (P= 0.710). Furthermore, the 4% HANP+MTA group continued to show significantly more new bone formation compared to control, 2% HANP+MTA, & 6% HANP+BC groups. These quantitative findings were consistent with the histopathological observations, where

 doi:10.20944/preprints202605.1131.v1

sections from the 4% HANP groups demonstrated reduced inflammatory cell infiltration and more organized tissue architecture compared with the other experimental groups, (Figures 5 and 6).

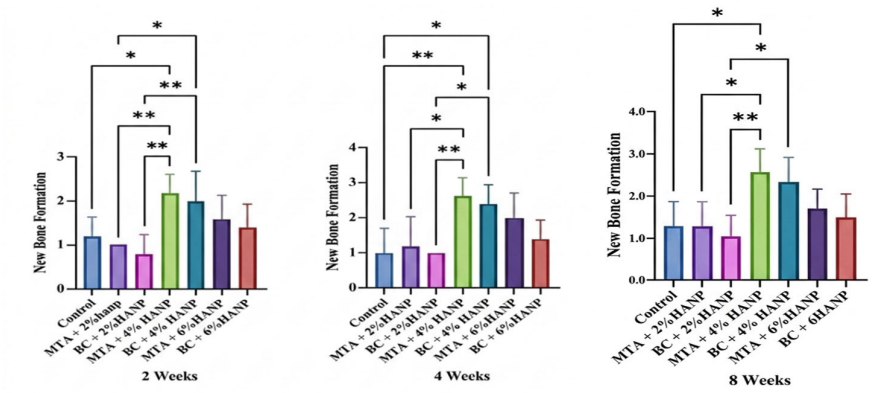

Figure 4. Pairwise comparison for new bone formation of control, MTA and BC sealer-modified with 2%,4% and 6% HANP at 2 Weeks, 4 Weeks and 8 Weeks intervals.

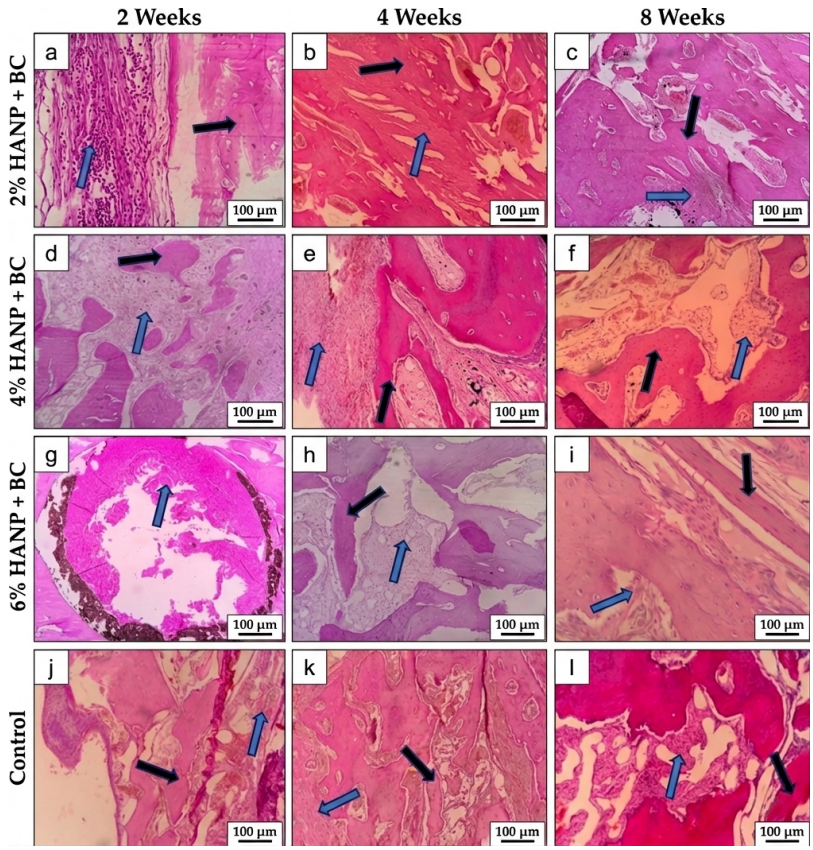

Figure 5. Representative hematoxylin and eosin (H&E)-stained histological sections showing bone regeneration and inflammatory response in defects treated with bioceramic (BC) sealer containing hydroxyapatite nanoparticles (HANP). Panels (a–c), 2% HANP + BC; (d–f), 4% HANP + BC; (g–i), 6% HANP + BC; and (j–l), control, evaluated at 2, 4, and 8 weeks. Black arrows indicate newly formed trabecular bone, and blue arrows indicate inflammatory cell infiltration. Magnification ×100.

 doi:10.20944/preprints202605.1131.v1

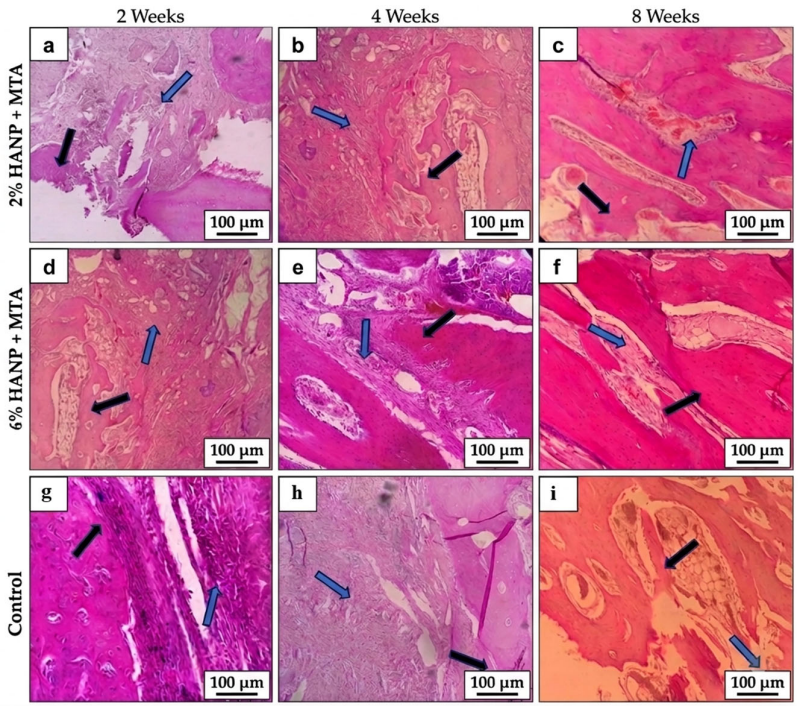

Figure 6. Representative hematoxylin and eosin (H&E)-stained histological sections showing bone regeneration and inflammatory response in defects treated with mineral trioxide aggregate (MTA) containing hydroxyapatite nanoparticles (HANP). Panels (a–c), 2% HANP + MTA; (d–f), 4% HANP + MTA; and (g–i), 6% HANP + MTA, evaluated at 2, 4, and 8 weeks. Black arrows indicate newly formed trabecular bone, and blue arrows indicate inflammatory cell infiltration. Magnification ×100.

3.3. Masson Trichrome Staining Results

The results show a progressive increase in collagen fiber deposition and maturation over time in all experimental groups, (Figures 7 and 8). At two weeks, the control group predominantly exhibited early immature collagen fibers arranged in a reticular pattern. Limited or low collagen deposition was observed in the 2% HANP groups, whereas the 4% HANP groups showed more organized collagen. In contrast, the 6% HANP + MTA group demonstrated minimal collagen deposition, while the 6% HANP + BC group presented mild collagen fiber formation.

At four weeks, collagen deposition increased in most groups, with moderate collagen bundles becoming more evident within the defect area. The 4% HANP groups demonstrated more pronounced collagen bundle formation compared with the other groups, whereas the control group continued to show only mild collagen fiber deposition. At eight weeks, further maturation of collagen fibers was observed, with several experimental groups demonstrating predominantly compact collagen bundles. The 4% HANP + MTA group exhibited the most advanced collagen organization, followed by the 4% HANP + BC group, while the 2% and 6% HANP groups showed moderate collagen maturation. The mean ± standard deviation (SD) values, along with median (IQR), of collagen fiber deposition and maturation around the implanted materials at the respective time intervals were presented in (Table 3).

 doi:10.20944/preprints202605.1131.v1

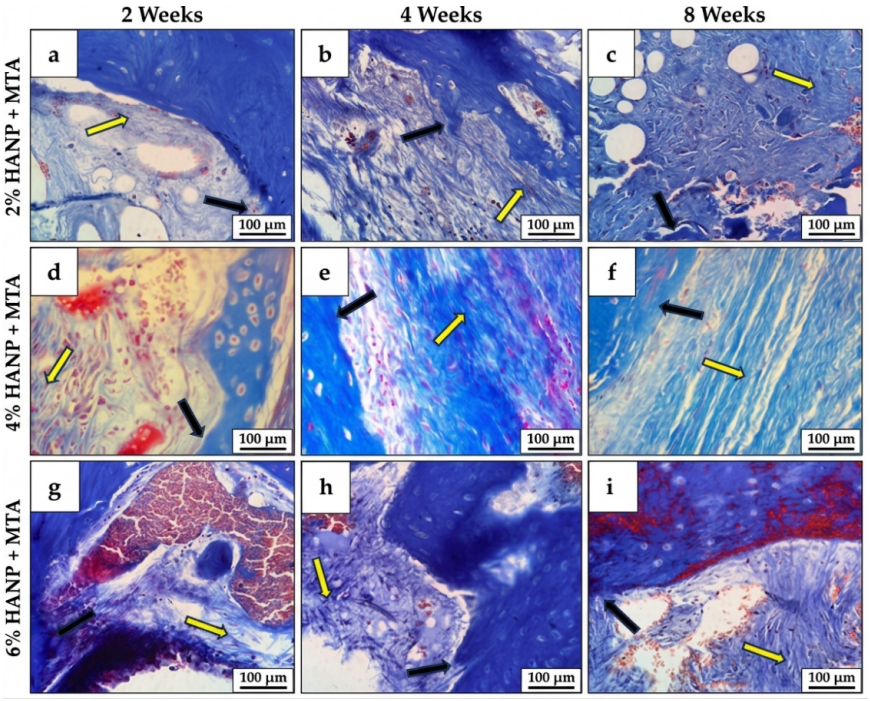

Figure 7. Representative Masson's trichrome-stained histological sections showing bone regeneration and collagen deposition in defects treated with mineral trioxide aggregate (MTA) containing hydroxyapatite nanoparticles (HANP). Panels (a–c) show 2% HANP + MTA, (d–f) 4% HANP + MTA, and (g–i) 6% HANP + MTA at 2, 4, and 8 weeks. Black arrows indicate newly formed bone trabeculae, and yellow arrows indicate collagen deposition. Magnification ×400.

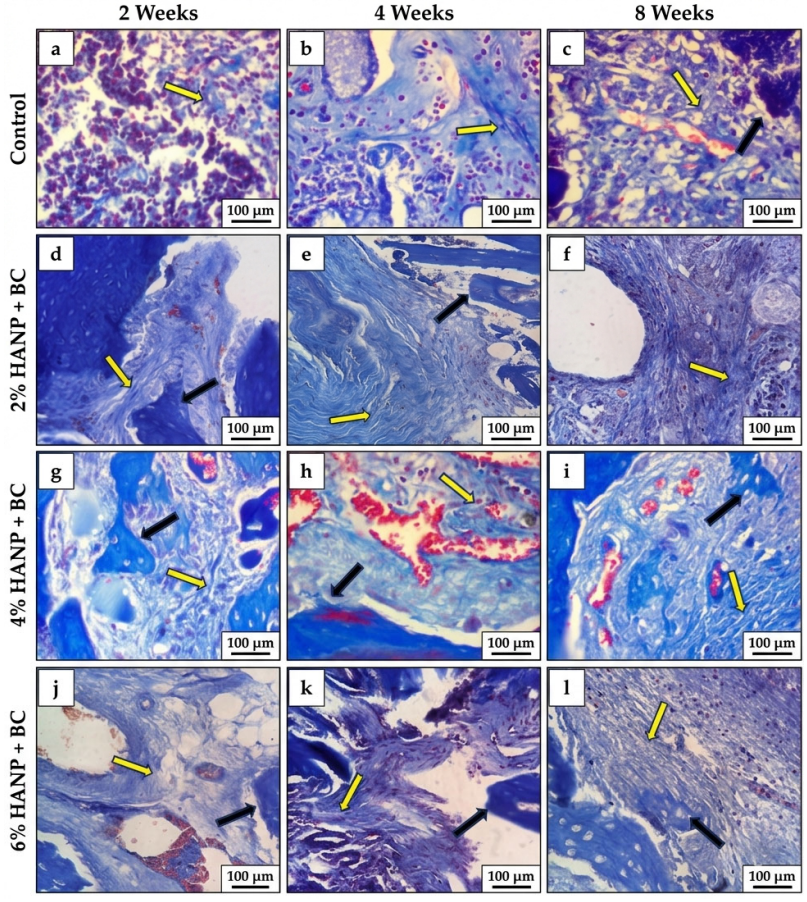

 doi:10.20944/preprints202605.1131.v1

Figure 8. Representative Masson's trichrome-stained histological sections showing bone regeneration and collagen deposition in control defects and defects treated with bioceramic (BC) sealer containing hydroxyapatite nanoparticles (HANP). Panels (a–c) show control, (d–f) 2% HANP + BC, (g–i) 4% HANP + BC, and (j–l) 6% HANP + BC at 2, 4, and 8 weeks. Black arrows indicate newly formed bone trabeculae, and yellow arrows indicate collagen deposition. Magnification ×400.

Table 3. Collagen fiber deposition scores (mean ± standard deviation and median [interquartile range]) in control and hydroxyapatite nanoparticle (HANP)-modified MTA and bioceramic (BC) groups at 2, 4, and 8 weeks.

Group	2 Weeks		4 Weeks		8 Weeks	
	(Mean ± SD)	**(Median [IQR])**	**(Mean ± SD)**	**(Median [IQR])**	**(Mean ± SD)**	**(Median [IQR])**
Control	0.00 ± 0.00^{a}	0 [0–0]	0.40 ± 0.55^{a}	0 [0–1]	1.00 ± 0.00^{a}	1 [1–1]
2% HANP + MTA	0.40 ± 0.55^{ab}	0 [0–1]	0.80 ± 0.45^{ab}	1 [1–1]	1.40 ± 0.55^{ab}	1 [1–2]
2% HANP + BC	0.20 ± 0.45^{a}	0 [0–0]	0.60 ± 0.55^{ab}	1 [0–1]	1.00 ± 0.00^{a}	1 [1–1]
4% HANP + MTA	1.00 ± 0.00^{c}	1 [1–1]	1.40 ± 0.55^{b}	1 [1–2]	2.00 ± 0.00^{c}	2 [2–2]
4% HANP + BC	1.00 ± 0.00^{bc}	1 [1–1]	1.20 ± 0.45^{b}	1 [1–1]	1.50 ± 0.55^{bc}	2 [1–2]
6% HANP + MTA	0.00 ± 0.00^{a}	0 [0–0]	1.00 ± 0.00^{ab}	1 [1–1]	1.40 ± 0.55^{ab}	1 [1–2]
6% HANP + BC	0.60 ± 0.55^{ab}	1 [0–1]	0.40 ± 0.55^{a}	0 [0–1]	1.20 ± 0.45^{ab}	1 [1–1]

(SD): standard deviation. Different superscript letters within the same column indicate statistically significant differences among groups ($p < 0.05$); values sharing at least one letter are not significantly different ($p \geq 0.05$).

For pairwise comparison of collagen fiber deposition among different groups using Bonferroni-adjusted pairwise comparison test. (Figure 9), shows that at 2 weeks, the 4% HANP+MTA group exhibited significantly higher collagen fiber deposition compared with control and 2% HANP+BC groups. Similarly, the 4% HANP+BC group demonstrated significantly greater collagen fiber formation as compared with the control group. In addition, the 6% HANP groups showed variable responses, with 6% HANP+BC demonstrating moderate collagen deposition, whereas 6% HANP+MTA exhibited minimal collagen formation comparable to the control group. However, no significant differences were detected between the two 4% HANP groups (MTA and BC) at 2 weeks ($p > 0.05$). The 4% HANP+MTA group exhibited the highest mean staining score at 4 week's intervals, indicating a greater degree of collagen maturation and extracellular matrix organization compared with the other groups. Statistical analysis showed that the 4% HANP+MTA group had significantly higher staining scores than the control group and the 6% HANP+BC group ($p < 0.05$). The 4% HANP+BC group also demonstrated relatively high collagen deposition, although its values were slightly lower than those of the 4% HANP+MTA group and the difference between these two groups was not statistically significant. At 8 weeks, the 4% HANP+MTA group demonstrated significantly greater collagen deposition compared with the control and 6% HANP+BC groups. Likewise, the 4% HANP+BC group exhibited significantly higher collagen maturation compared with the control group. However, non-significant differences were detected between both 4% HANP groups and among the remaining studied group ($p > 0.05$).

 doi:10.20944/preprints202605.1131.v1

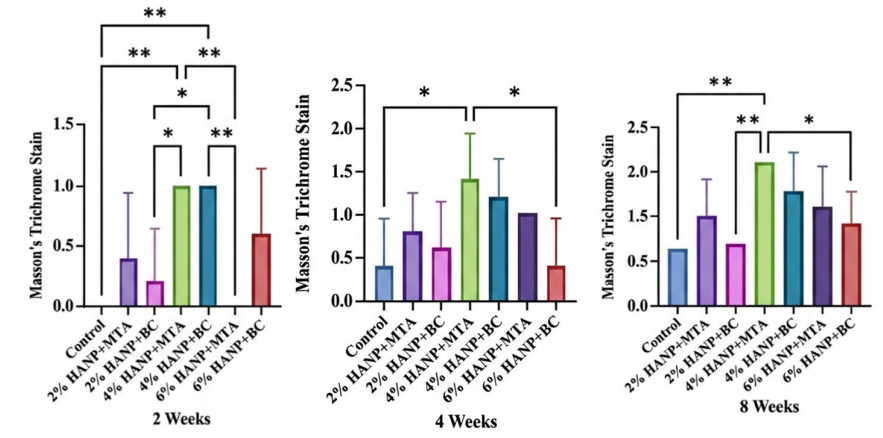

Figure 9. Pairwise comparison for Masson's trichrome stain of control, MTA and BC sealer-modified with 2%,4% and 6% HANP at 2 Weeks, 4 Weeks, 8 Weeks intervals.

4. Discussion

The present study demonstrated that the incorporation of nano-hydroxyapatite (HANP) into mineral trioxide aggregate (MTA) and bioceramic (BC) sealers significantly influences bone regeneration in a concentration-dependent manner. Among the tested formulations, the 4% HANP concentration provided the most favorable balance between enhanced new bone formation and reduced inflammatory response. Histological findings across all observation periods confirmed that both the material composition and nanoparticle concentration are critical determinants of in vivo tissue healing outcomes. Hydroxyapatite-based biomaterials are widely recognized for their osteoconductive properties and their ability to support bone regeneration. In particular, nano-hydroxyapatite (HANP) has gained increasing attention due to its high surface area and close resemblance to the mineral phase of natural bone, which enhances cellular interactions and promotes osteoblast activity and matrix mineralization [30]. Clinical and preclinical evidence further supports the use of nanocrystalline hydroxyapatite as an effective bone substitute, demonstrating improved bone regeneration outcomes comparable to conventional graft materials [31]. However, despite these advantages, the biological response to HANP is highly dependent on its physicochemical characteristics and concentration. Variations in nanoparticle size, structure, and surface properties can modulate inflammatory responses and cellular behavior, potentially leading to either enhanced healing or undesirable tissue reactions [32]. This highlights a critical gap in current knowledge regarding the optimal concentration of HANP, particularly when incorporated into bioactive endodontic materials.

Mineral trioxide aggregate (MTA) and bioceramic (BC) sealers are extensively used in endodontics due to their sealing ability and inherent bioactivity, including the capacity to induce hard tissue formation. Nevertheless, their regenerative performance can still be optimized, especially in terms of accelerating bone formation and modulating inflammation. The incorporation of HANP into these materials represents a promising strategy to enhance their osteogenic potential, as composite nano-hydroxyapatite-based systems have been shown to further stimulate bone regeneration compared to conventional materials alone [33]. Accordingly, the present study aimed to address the lack of consensus regarding the most effective HANP concentration by systematically evaluating its incorporation into MTA and BC sealers.

The rabbit model is widely utilized in craniofacial bone regeneration research, including maxillary and alveolar bone defect studies, due to its anatomical suitability and translational relevance to dental applications. Experimental models in rabbits allow the evaluation of bone substitutes in both cranial (non-load-bearing) and alveolar or mandibular (load-bearing) regions, which exhibit distinct healing characteristics relevant to maxillofacial reconstruction [34].

 doi:10.20944/preprints202605.1131.v1

The present findings demonstrate that inflammatory cell infiltration is strongly influenced by both nano-hydroxyapatite (HANP) concentration and healing time, exhibiting clear concentration- and time-dependent trends. The elevated inflammatory response observed at 2 weeks across most groups reflects the expected acute inflammatory phase following biomaterial implantation, which is essential for initiating tissue repair and regeneration. This response is consistent with established evidence indicating that early leukocyte recruitment and macrophage activation are critical regulators of healing outcomes and biomaterial integration [32]. A progressive reduction in inflammation at 4 and 8 weeks further supports the pivotal role of time in the resolution of the inflammatory process, in agreement with previous reports [35]

The pronounced early inflammatory response may also be partially attributed to the intrinsic properties of the base materials. Calcium silicate–based sealers are characterized by a high alkaline pH, which can stimulate the release of pro-inflammatory cytokines, including IL-1 and IL-6, during the initial healing phase [36]. In addition, their relatively delayed setting time allows maintenance of an elevated pH (up to ~12) for an extended period, enhancing antimicrobial activity while potentially prolonging tissue irritation [37]. Thermal changes associated with the setting reaction may further contribute to inflammatory cell recruitment and cytokine release [38].

Notably, the 4% HANP groups exhibited a consistently reduced inflammatory response at all-time points, suggesting a concentration-dependent immunomodulatory effect. This phenomenon may be explained by the ability of nano-hydroxyapatite to regulate macrophage polarization. Macrophages play a central role in inflammation by transitioning between the pro-inflammatory M1 phenotype and the anti-inflammatory, reparative M2 phenotype. Evidence indicates that HANP promotes M2 polarization while suppressing M1 activity [39]. Therefore, the 4% concentration may have established a microenvironment favoring M2 dominance, thereby facilitating resolution of inflammation and progression toward tissue regeneration. In contrast, both lower (2%) and higher (6%) concentrations appear less effective in achieving this balance, resulting in relatively increased inflammatory responses.

The superior performance of the 4% HANP groups further suggests that this concentration achieves an optimal balance between bioactivity and biocompatibility. This observation is consistent with previous experimental and clinical studies demonstrating that nano-hydroxyapatite can modulate key inflammatory mediators, such as interleukin-1β (IL-1β) and tumor necrosis factor-α (TNF-α), thereby reducing inflammatory burden and enhancing healing outcomes [40].

In contrast, the increased inflammatory response observed in the 2% HANP-modified groups indicates that this concentration is insufficient to induce effective bioactive and immunomodulatory effects. At low nanoparticle loading, the release of calcium and phosphate ions may not reach the threshold required to regulate macrophage behavior or promote the transition from an M1 to an M2 phenotype, leading to sustained inflammatory cell infiltration. Additionally, limited HANP incorporation may inadequately modify surface properties and sealing ability, thereby impairing protein adsorption, cell adhesion, and interfacial stability—factors essential for early inflammation resolution. This interpretation aligns with previous findings that the biological performance of nano-hydroxyapatite is highly concentration-dependent, with suboptimal concentrations failing to enhance bioactivity or modulate inflammation effectively [41].

Conversely, higher nanoparticle loading (6% HANP-modified groups) may introduce an excessive particulate burden that exacerbates early inflammatory responses. This may be attributed to increased macrophage activation and elevated expression of pro-inflammatory cytokines, resulting in prolonged inflammation and delayed healing [42].

The absence of significant differences between MTA- and BC-based materials within the 4% HANP groups further suggests that nanoparticle concentration plays a more critical role than the base material in determining the inflammatory outcome. This interpretation is supported by evidence indicating that calcium silicate–based sealers, including both MTA and bioceramic formulations, exhibit broadly comparable biocompatibility and tend to show reduced inflammatory responses over time, with differences often being material-specific but not always statistically significant [43].

 doi:10.20944/preprints202605.1131.v1

The present study employed nano-hydroxyapatite (HANP) due to its well-documented osteoconductive properties and ability to enhance early bone remodeling. Previous studies have demonstrated that HANP promotes significantly greater bone formation compared to conventional biomaterials such as standard hydroxyapatite, tricalcium phosphate, and gelatin-based scaffolds [44–46]. This enhanced osteogenic potential has been partly attributed to the structural characteristics of HANP, particularly its porosity, which plays a critical role in both early and late stages of osteogenesis by facilitating cellular infiltration and vascularization, as proposed by Habibovic et al. [47]. Supporting evidence from both animal and human studies further indicates that pore size and interconnectivity significantly influence bone regeneration by promoting angiogenesis and tissue ingrowth [48].

In the present study, new bone formation increased progressively over time, demonstrating a clear concentration-dependent pattern influenced by both HANP content and material type. Among all groups, the 4% HANP formulation exhibited superior outcomes, characterized by enhanced trabecular organization, denser mineralized tissue deposition, and more continuous defect bridging compared with both lower (2%) and higher (6%) concentrations. These findings are consistent with previous evidence indicating that optimally dosed hydroxyapatite nanoparticles enhance osteoblast adhesion, proliferation, and mineralization due to their nanoscale topography and chemical similarity to native bone mineral [49]. In contrast, lower concentrations may provide insufficient surface area for effective cell–material interaction, while higher concentrations may adversely affect material porosity and setting characteristics, thereby compromising biological performance [50].

The enhanced osteogenesis observed in the 4% HANP groups may also be attributed to increased alkaline phosphatase activity, which plays a key role in matrix mineralization. HANP provides a favorable scaffold for osteoprogenitor cell attachment and differentiation, thereby promoting early osteoid deposition and subsequent maturation of bone tissue [51]. Additionally, the nanoscale architecture and interconnectivity of HANP may facilitate angiogenesis and cell migration even in the absence of exogenous growth factors, further supporting defect repair and bone regeneration [52]. Collectively, these mechanisms may explain the superior osteogenic performance observed at the 4% concentration. In contrast, the control group demonstrated only moderate increases in bone formation over time, reflecting the limited regenerative capacity of untreated bone defects, as reported in previous animal studies [53].

The present findings are in agreement with prior in vivo studies demonstrating that HANP incorporation enhances early recruitment and differentiation of osteoprogenitor cells, leading to accelerated matrix deposition and maturation within defect sites [54]. The significant intergroup differences observed at later time points further confirm that HANP incorporation improves defect bridging, osteointegration, and overall bone regeneration without inducing adverse inflammatory responses [55]. Similar outcomes have been reported by Kubasiewicz et al. (2017), who demonstrated that HANP, either alone or in combination with other biomaterials, significantly enhances bone regeneration compared to untreated defects [56].

Importantly, no statistically significant differences were observed between HANP-modified mineral trioxide aggregate (MTA) and bioceramic (BC) groups in terms of new bone formation over time. This may be attributed to the similar physicochemical and biological properties of calcium silicate–based materials. Both MTA and BC release calcium and hydroxyl ions during hydration, creating an alkaline environment that promotes hydroxyapatite formation, mineralization, and tissue regeneration [57]. Their osteogenic potential has also been linked to their ability to stimulate angiogenesis and support osteoblastic differentiation through the release of bioactive ions [58]. Consistent with these findings, Rifaey et al. (2016), reported that bioceramic materials enhance osteoblastic differentiation in three-dimensional culture systems [59]. while multiple studies have confirmed the capacity of MTA to promote new bone formation, as evidenced by active osteoblasts, collagen deposition, and mineralized matrix formation at defect sites [60,61].

For enhanced histological evaluation, Masson's trichrome staining was employed to assess both the extent of newly formed bone and the quality of its mineralization across the experimental groups.

 doi:10.20944/preprints202605.1131.v1

This approach is widely used in bone defect studies to differentiate between immature fibrous tissue and mature mineralized bone, thereby providing insight into the progression of tissue repair [62].

The findings of the present study demonstrated a clear concentration-dependent effect of nano-hydroxyapatite (HANP) on bone regeneration, with the 4% HANP-modified mineral trioxide aggregate (MTA) and bioceramic (BC) groups showing optimal outcomes. This observation is consistent with previous reports indicating that HANP, when homogeneously distributed within a scaffold or matrix, closely mimics the mineral phase of native bone. Such biomimetic properties enhance osteogenic cell adhesion, proliferation, and subsequent matrix mineralization. The increased collagen deposition and mineralized matrix observed in Masson's trichrome-stained sections further support the role of HANP in promoting osteogenic differentiation and extracellular matrix (ECM) maturation [30].

At the early healing stage (2 weeks), the control group predominantly exhibited immature, reticular collagen, whereas the 4% HANP groups demonstrated more organized collagen architecture with higher semiquantitative scores. This early enhancement in collagen organization may reflect accelerated formation of a provisional matrix conducive to osteoid deposition and subsequent remodeling. The bioactivity of calcium silicate–based materials, including their ability to release calcium ions, elevate local pH, and form an apatite-like layer, may further contribute to early extracellular matrix organization and osteogenic cellular responses, particularly in the 4% HANP groups [63].

By 4 weeks, collagen fiber deposition increased across most groups, with the 4% HANP + MTA group exhibiting the highest mean values and significant differences compared to the control and 6% HANP + BC groups. This trend aligns with previous in vitro findings demonstrating that calcium silicate–based materials support sustained matrix maturation through continuous ion release and surface mineral deposition, thereby promoting osteoblast differentiation and matrix formation [64].

At 8 weeks, most treated groups exhibited predominantly dense and well-organized collagen bundles, indicative of advanced extracellular matrix maturation. The 4% HANP groups continued to show superior outcomes, with significant differences compared to the control group, and the 4% HANP + MTA group demonstrating enhanced collagen deposition relative to the 6% HANP + BC group. This progressive organization reflects the natural remodeling process of bone healing, in which immature collagen is gradually replaced by thicker, more aligned fibers that serve as a scaffold for mineral deposition and tissue consolidation. These findings are consistent with previous studies linking increased collagen organization at later stages with enhanced matrix maturation and bone regeneration [65,66].

The superior collagen deposition and organization observed in the 4% HANP groups, compared to both 2% and 6% concentrations, likely reflect an optimal balance between nanoparticle availability and biological activity. At lower concentrations (2%), insufficient nanoparticle surface area may limit protein adsorption, cell attachment, and nucleation sites for apatite formation, resulting in only modest improvements over control conditions [67]. Conversely, higher concentrations (6%) may lead to nanoparticle agglomeration, reducing effective surface area and altering cell–material interactions, thereby diminishing biological performance. This phenomenon has been well documented for hydroxyapatite nanoparticles, which tend to aggregate under certain conditions, ultimately affecting their regenerative potential [68].

Taken together, the histological, histomorphometric, and Masson's trichrome findings of the present study demonstrate that nano-hydroxyapatite (HANP)-modified calcium silicate–based materials significantly enhance bone regeneration in maxillary bone defects in a concentration-dependent manner. Among the tested formulations, the 4% HANP groups consistently exhibited the most favorable outcomes, characterized by reduced inflammatory response, enhanced collagen organization, and increased new bone formation. These findings highlight the interplay between inflammation modulation and osteogenesis during the healing process and underscore the importance of optimizing nanoparticle concentration to achieve a balance between bioactivity and biocompatibility.

 doi:10.20944/preprints202605.1131.v1

The results further suggest that HANP incorporation not only promotes osteoconduction but may also regulate the local biological environment to favor tissue regeneration. Future studies should incorporate advanced three-dimensional imaging techniques, such as micro-computed tomography (micro-CT), to enable more precise quantification of bone volume and microarchitecture. In addition, molecular and immunohistochemical analyses targeting inflammatory mediators, macrophage polarization, and osteogenic markers would provide deeper insight into the mechanisms underlying the observed effects. Longer observation periods are also recommended to evaluate the long-term maturation, remodeling, and functional stability of the regenerated bone.

5. Conclusions

Within the limitations of the present study, the incorporation of nano-hydroxyapatite significantly enhanced the biological performance of calcium silicate–based sealers in a concentration-dependent manner. The 4% HANP formulation demonstrated the most favorable balance, characterized by reduced inflammatory response, increased new bone formation, and improved collagen maturation. No statistically significant differences were observed between mineral trioxide aggregate (MTA) and bioceramic (BC) sealers at equivalent HANP concentrations, indicating comparable biological behavior. Collectively, these findings identify 4% HANP-modified calcium silicate sealers as promising biomaterials for bone regeneration and support their potential application in regenerative bone repair.

Author Contributions: Conceptualization, A.A.A; methodology, A.A.A; validation, B.K.A; formal analysis, A.A.A; investigation, A.A.A; data curation, A.A.A; writing—original draft preparation, A.A.A; writing—review and editing, C.A.M and B.K.A; visualization, A.A.A; supervision, C.A.M and B.K.A; project administration, A.A.A. All authors have read and agreed to the published version of the manuscript.

Funding: This research received no external funding.

Institutional Review Board Statement: The present animal study was approved by the Research Ethic Committee of the College of Dentistry, Hawler Medical University, Erbil, Kurdistan Region-Iraq (reference No: HMUD,2425057, approved on 22 December 2024). All procedures were conducted in accordance with ARRIVE (Animal Research: Reporting of In Vivo Experiments) guideline and institutional regulations for animal care and use.

Data Availability Statement: The datasets generated and analyzed during the present study, including histological images and histomorphometric measurements, are available from corresponding author up on reasonable request.

Acknowledgments: The authors express their deep appreciation and sincere thanks to the staff of the animal research facility and the laboratory team at Hawler Medical University for their valuable assistance during the experimental procedure in conducting the laboratory work and histological preparation. The authors also extend their gratitude to the Department of Periodontics and Conservative Dentistry, College of Dentistry, Hawler Medical University for their support.

Conflicts of Interest: The authors declare no conflicts of interest.

Abbreviations

The following abbreviations are used in this manuscript:

BC	Bioceramic sealer
BM	Body weight
DPX	Dibutyl phthalate polystyrene xylene
ECM	Extracellular matrix
HANP	Hydroxyapatite nanoparticles
IL-1	Interleukin-1
IL-6	Interleukin-6

 doi:10.20944/preprints202605.1131.v1

M1	Pro-inflammatory macrophages
M2	Anti-inflammatory macrophages
MT	Masson's trichrome
MTA	Mineral trioxide aggregate
RunX2	Runt-related transcription factor 2
SD	Standard deviation
TGF-β	Transforming growth factor beta

References

1. Xiang H, Wang Y, Chang H, Yang S, Tu M, Zhang X, et al. Cerium-containing α-calcium sulfate hemihydrate bone substitute promotes osteogenesis. Journal of biomaterials applications. 2019;34(2):250-60.
2. Chen Y, Zhou Y, Yang S, Li JJ, Li X, Ma Y, et al. Novel bone substitute composed of chitosan and strontium-doped α-calcium sulfate hemihydrate: Fabrication, characterisation and evaluation of biocompatibility. Materials science & engineering C, Materials for biological applications. 2016;66:84-91.
3. Liu Z, Yu Z, Chang H, Wang Y, Xiang H, Zhang X, et al. Strontium-containing α-calcium sulfate hemihydrate promotes bone repair via the TGF-β/Smad signaling pathway. Molecular medicine reports. 2019;20(4):3555-64.
4. Leventis M, Fairbairn P, Mangham C, Galanos A, Vasiliadis O, Papavasileiou D, et al. Bone healing in rabbit calvaria defects using a synthetic bone substitute: a histological and micro-CT comparative study. Materials. 2018;11(10):2004.
5. Yamada M, Egusa H. Current bone substitutes for implant dentistry. Journal of prosthodontic research. 2018;62(2):152-61.
6. Sohn HS, Oh JK. Review of bone graft and bone substitutes with an emphasis on fracture surgeries. Biomaterials research. 2019;23:9.
7. Lobb DC, DeGeorge BR, Jr., Chhabra AB. Bone Graft Substitutes: Current Concepts and Future Expectations. The Journal of hand surgery. 2019;44(6):497-505.e2.
8. Yang S, Wang L, Feng S, Yang Q, Yu B, Tu M. Enhanced bone formation by strontium modified calcium sulfate hemihydrate in ovariectomized rat critical-size calvarial defects. Biomedical Materials. 2017;12(3):035004.
9. Pförringer D, Harrasser N, Mühlhofer H, Kiokekli M, Stemberger A, van Griensven M, et al. Osteoinduction and -conduction through absorbable bone substitute materials based on calcium sulfate: in vivo biological behavior in a rabbit model. Journal of materials science Materials in medicine. 2018;29(2):17.
10. Fernandez de Grado G, Keller L, Idoux-Gillet Y, Wagner Q, Musset A-M, Benkirane-Jessel N, et al. Bone substitutes: a review of their characteristics, clinical use, and perspectives for large bone defects management. Journal of tissue engineering. 2018;9:2041731418776819.
11. Sánchez-Garcés MÁ, Camps-Font O, Escoda-Francolí J, Muñoz-Guzón F, Toledano-Serrabona J, Gay-Escoda C. Short time guided bone regeneration using beta-tricalcium phosphate with and without fibronectin–An experimental study in rats. Medicina Oral, Patología Oral y Cirugía Bucal. 2020;25(4):e532.
12. Mohd Zaffarin AS, Ng S-F, Ng MH, Hassan H, Alias E. Nano-hydroxyapatite as a delivery system for promoting bone regeneration in vivo: a systematic review. Nanomaterials. 2021;11(10):2569.
13. Eskandarinezhad M, Ghodrati M, Pournaghi Azar F, Jafari F, Samadi Pakchin P, Abdollahi AA, et al. Effect of Incorporating Hydroxyapatite and Zinc Oxide Nanoparticles on the Compressive Strength of White Mineral Trioxide Aggregate. Journal of dentistry (Shiraz, Iran). 2020;21(4):300-6.
14. Agha BH, Hamasaeed NH, Hussain FH. Novel incorporation of charged hydroxyapatite nanoparticles into resin adhesive. Cellular and Molecular Biology. 2023;69(11):149-54.
15. Ahirwar H, Zhou Y, Mahapatra C, Ramakrishna S, Kumar P, Nanda HS. Materials for orthopedic bioimplants: modulating degradation and surface modification using integrated nanomaterials. Coatings. 2020;10(3):264.
16. Paz JER, Costa PO, Souza AAC, de Oliveira IM, Falcão LF, Falcão CAM, et al. Bone repair in defects filled with AH Plus sealer and different concentrations of MTA: a study in rat tibiae. Restorative Dentistry & Endodontics. 2021;46(4).

 doi:10.20944/preprints202605.1131.v1

17. Galal GM, Abd El Rehim SS, Karam SS. The effect of mineral trioxide aggregate alone and in combination with biphasic calcium phosphate on healing of mandibular defects in rabbit. Alexandria Dental Journal. 2019;44(3):77-81.
18. Miller AA, Takimoto K, Wealleans J, Diogenes A. Effect of 3 bioceramic materials on stem cells of the apical papilla proliferation and differentiation using a dentin disk model. Journal of endodontics. 2018;44(4):599-603.
19. Abdulhaq AA, Anwar Mohammad C, Karim Amin B. Physiochemical Characterization of Hydroxyapatite Nanoparticle-Modified Mineral Trioxide Aggregate and Bioceramic Sealers. Journal of Nanostructures. 2025;15(4):1885-900.
20. Alsaeed MA, Al-Ghaban NM. Chitosan Nanoparticle/Simvastatin for Experimental Maxillary Bony Defect Healing: A Histological and Histomorphometrical Study. Biomimetics. 2023;8(4):363.
21. Al-Shamaa RM, Al-Askary RA. Remineralizing capacity of zinc oxide eugenol sealer following the addition of nanohydroxyapatite-tyrosine amino acid: An in vivo animal study. Journal of Oral Biosciences. 2025;67(1):100567.
22. Miquelestorena-Standley E, Jourdan ML, Collin C, Bouvier C, Larousserie F, Aubert S, et al. Effect of decalcification protocols on immunohistochemistry and molecular analyses of bone samples. Modern pathology : an official journal of the United States and Canadian Academy of Pathology, Inc. 2020;33(8):1505-17.
23. Fadhil E, Dosh RH, Wally ZJ, Haider J. Histological evaluation of the effects of bone morphogenetic protein 9 and angiopoietin 1 on bone healing. Journal of Taibah University Medical Sciences. 2023;18(5):954-63.
24. Hagh LG, Karimi B, Moghimipour E, Abdi Z, Abdolalian F, Rohani A. Histological evaluation of wound healing effect of topical phenytoin on rat hard palate mucosa. Journal of Research in Medical and Dental Science. 2018;6(2):466-72.
25. Al-Askary RA, Al-Ashou WMO, Al-Jubori SH. Remineralization ability of different root canal sealers. The Saudi dental journal. 2023;35(8):1014-22.
26. Moraes PC, Marques ICS, Basso FG, Rossetto HL, Pires-de-Souza FCP, Costa CAS, et al. Repair of Bone Defects with Chitosan-Collagen Biomembrane and Scaffold Containing Calcium Aluminate Cement. Brazilian dental journal. 2017;28(3):287-95.
27. Mohammad CA, Ali KM, Al-Rawi RA, Gul SS. Effects of curcumin and tetracycline gel on experimental induced periodontitis as an anti-inflammatory, osteogenesis promoter and enhanced bone density through altered Iron levels: histopathological study. Antibiotics. 2022;11(4):521.
28. Jeong JH, Jin E-S, Kim JY, Min J, Jeon SR, Lee M, et al. Bone formation effect of highly concentrated tricalcium phosphate biocomposite screws in a rabbit osteoporosis model. Journal of Orthopaedic Research. 2022;40(6):1321-8.
29. da Silva Brum I, Frigo L, Lana Devita R, da Silva Pires JL, Hugo Vieira de Oliveira V, Rosa Nascimento AL, et al. Histomorphometric, Immunohistochemical, Ultrastructural Characterization of a Nano-Hydroxyapatite/Beta-Tricalcium Phosphate Composite and a Bone Xenograft in Sub-Critical Size Bone Defect in Rat Calvaria. Materials (Basel, Switzerland). 2020;13(20).
30. Hoveidaei AH, Sadat-Shojai M, Mosalamiaghili S, Salarikia SR, Roghani-Shahraki H, Ghaderpanah R, et al. Nano-hydroxyapatite structures for bone regenerative medicine: Cell-material interaction. Bone. 2024;179:116956.
31. Shaheen MY. Nanocrystalline hydroxyapatite in periodontal bone regeneration: A systematic review. The Saudi dental journal. 2022;34(8):647-60.
32. Mestres G, Espanol M, Xia W, Persson C, Ginebra MP, Ott MK. Inflammatory response to nano- and microstructured hydroxyapatite. PLoS One. 2015;10(3):e0120381.
33. Mitić D, Čarkić J, Jaćimović J, Lazarević M, Jakšić Karišik M, Toljić B, et al. The Impact of Nano-Hydroxyapatite Scaffold Enrichment on Bone Regeneration In Vivo-A Systematic Review. Biomimetics (Basel, Switzerland). 2024;9(7).
34. Schlund M, Depeyre A, Kotagudda Ranganath S, Marchandise P, Ferri J, Chai F. Rabbit calvarial and mandibular critical-sized bone defects as an experimental model for the evaluation of craniofacial bone tissue regeneration. Journal of Stomatology, Oral and Maxillofacial Surgery. 2022;123(6):601-9.

 doi:10.20944/preprints202605.1131.v1

35. Tavares CO, Böttcher DE, Assmann E, Kopper PM, de Figueiredo JA, Grecca FS, et al. Tissue reactions to a new mineral trioxide aggregate-containing endodontic sealer. Journal of endodontics. 2013;39(5):653-7.
36. Torabinejad M, Parirokh M. Mineral trioxide aggregate: a comprehensive literature review--part II: leakage and biocompatibility investigations. J Endod. 2010;36(2):190-202.
37. Elsayed MA, Elgendy AA, Hassanien IE, Schäfer E. Evaluation of osteoconductivity and inflammatory response of a resin-based and a resin-free calcium silicate sealer: an in vivo study. Clinical Oral Investigations. 2025;29(6):334.
38. Zaki DY, Zaazou MH, Khallaf ME, Hamdy TM. In Vivo Comparative Evaluation of Periapical Healing in Response to a Calcium Silicate and Calcium Hydroxide Based Endodontic Sealers. Open access Macedonian journal of medical sciences. 2018;6(8):1475-9.
39. Linares J, Fernández AB, Feito MJ, Matesanz MC, Sánchez-Salcedo S, Arcos D, et al. Effects of nanocrystalline hydroxyapatites on macrophage polarization. Journal of Materials Chemistry B. 2016;4(11):1951-9.
40. Xie H, Tan A, Su Z, Pan C, Li S, Xiao H. Effect of nano-hydroxyapatite filling on masticatory function and gingival sulcular fluid inflammatory factor levels in periapical inflammation. BioMedical Engineering OnLine. 2025;24(1):63.
41. Xiao L, Shiwaku Y, Hamai R, Tsuchiya K, Sasaki K, Suzuki O. Macrophage Polarization Related to Crystal Phases of Calcium Phosphate Biomaterials. International journal of molecular sciences. 2021;22(20).
42. Shi Z, Huang X, Cai Y, Tang R, Yang D. Size effect of hydroxyapatite nanoparticles on proliferation and apoptosis of osteoblast-like cells. Acta biomaterialia. 2009;5(1):338-45.
43. Yang X, Tian J, Li M, Chen W, Liu H, Wang Z, et al. Biocompatibility of a New Calcium Silicate-Based Root Canal Sealer Mediated via the Modulation of Macrophage Polarization in a Rat Model. Materials (Basel, Switzerland). 2022;15(5).
44. Henkel KO, Gerber T, Lenz S, Gundlach KK, Bienengräber V. Macroscopical, histological, and morphometric studies of porous bone-replacement materials in minipigs 8 months after implantation. Oral surgery, oral medicine, oral pathology, oral radiology, and endodontics. 2006;102(5):606-13.
45. Oltramari PVP, de Lima Navarro R, Henriques JFC, Taga R, Cestari TM, Ceolin DS, et al. Orthodontic movement in bone defects filled with xenogenic graft: an experimental study in minipigs. American Journal of Orthodontics and Dentofacial Orthopedics. 2007;131(3):302. e10-. e17.
46. Gamal SMM, Bilal MM, Soheir El-Sayed El S. Evaluation of the effectiveness of hyaluronic acid plus nanohydroxyapatite versus nanohydroxyapatite alone on bone regeneration in rabbits. Tanta Dental Journal. 2022;19(2):77-83.
47. Habibovic P, Sees TM, van den Doel MA, van Blitterswijk CA, de Groot K. Osteoinduction by biomaterials—physicochemical and structural influences. Journal of Biomedical Materials Research Part A: An Official Journal of The Society for Biomaterials, The Japanese Society for Biomaterials, and The Australian Society for Biomaterials and the Korean Society for Biomaterials. 2006;77(4):747-62.
48. Götz W, Gerber T, Michel B, Lossdörfer S, Henkel KO, Heinemann F. Immunohistochemical characterization of nanocrystalline hydroxyapatite silica gel (NanoBone(r)) osteogenesis: a study on biopsies from human jaws. Clinical oral implants research. 2008;19(10):1016-26.
49. Tzavellas A-N, Katrilaka C, Karipidou N, Kanari M, Pitou M, Koliakos G, et al. The "Forgotten" Hydroxyapatite Crystals in Regenerative Bone Tissue Engineering: A Critical Review. Crystals. 2024;14(5):448.
50. Sonowal L, Gautam S, Mambiri LT, Depan D. Advancements of bioceramics in biomedical applications. Next Materials. 2025.
51. Götz W, Lenz S, Reichert C, Henkel KO, Bienengräber V, Pernicka L, et al. A preliminary study in osteoinduction by a nano-crystalline hydroxyapatite in the mini pig. Folia histochemica et cytobiologica. 2010;48(4):589-96.
52. Furuya H, Tabata Y, Kaneko K. Bone regeneration for murine femur fracture by gelatin hydrogels incorporating basic fibroblast growth factor with different release profiles. Tissue engineering Part A. 2014;20(9-10):1531-41.

 doi:10.20944/preprints202605.1131.v1

53. Percival KM, Paul V, Husseini GA. Recent Advancements in Bone Tissue Engineering: Integrating Smart Scaffold Technologies and Bio-Responsive Systems for Enhanced Regeneration. International journal of molecular sciences. 2024;25(11).
54. El-Bahrawy NR, Hafez A, Elmekawy A, Salem M, Sarhan N, Morsy R. Development and characterization of nano-hydroxyapatite/gelatin/PVA/alginate-based multifunctional active scaffolds for bone regeneration: An in vitro and in vivo study. International journal of biological macromolecules. 2025;307(Pt 2):141160.
55. Zhao R, Meng X, Pan Z, Li Y, Qian H, Zhu X, et al. Advancements in nanohydroxyapatite: synthesis, biomedical applications and composite developments. Regenerative biomaterials. 2025;12:rbae129.
56. Kubasiewicz-Ross P, Hadzik J, Seeliger J, Kozak K, Jurczyszyn K, Gerber H, et al. New nano-hydroxyapatite in bone defect regeneration: A histological study in rats. Annals of anatomy = Anatomischer Anzeiger : official organ of the Anatomische Gesellschaft. 2017;213:83-90.
57. Dong X, Xu X. Bioceramics in Endodontics: Updates and Future Perspectives. Bioengineering (Basel, Switzerland). 2023;10(3).
58. Zordan-Bronzel CL, Tanomaru-Filho M, Rodrigues EM, Chávez-Andrade GM, Faria G, Guerreiro-Tanomaru JM. Cytocompatibility, bioactive potential and antimicrobial activity of an experimental calcium silicate-based endodontic sealer. International endodontic journal. 2019;52(7):979-86.
59. Rifaey HS, Villa M, Zhu Q, Wang YH, Safavi K, Chen IP. Comparison of the Osteogenic Potential of Mineral Trioxide Aggregate and Endosequence Root Repair Material in a 3-dimensional Culture System. Journal of endodontics. 2016;42(5):760-5.
60. Moretton TR, Brown CE, Jr., Legan JJ, Kafrawy AH. Tissue reactions after subcutaneous and intraosseous implantation of mineral trioxide aggregate and ethoxybenzoic acid cement. Journal of biomedical materials research. 2000;52(3):528-33.
61. Camilleri J, Atmeh A, Li X, Meschi N. Present status and future directions: Hydraulic materials for endodontic use. International endodontic journal. 2022;55 Suppl 3(Suppl 3):710-77.
62. El Halawany M, Saleh HA, Khashaba M, AbouGhaly MHH, Latif R. The effect of tranexamic acid-loaded alginate scaffolds on bone formation: hemostatic and histomorphometric analysis in a rabbit model. Future Journal of Pharmaceutical Sciences. 2025;11(1):99.
63. Primus CM, Tay FR, Niu LN. Bioactive tri/dicalcium silicate cements for treatment of pulpal and periapical tissues. Acta biomaterialia. 2019;96:35-54.
64. Song W, Sun W, Chen L, Yuan Z. In vivo Biocompatibility and Bioactivity of Calcium Silicate-Based Bioceramics in Endodontics. Frontiers in bioengineering and biotechnology. 2020;8:580954.
65. Garnero P. The contribution of collagen crosslinks to bone strength. BoneKEy reports. 2012;1:182.
66. Reznikov N, Shahar R, Weiner S. Three-dimensional structure of human lamellar bone: the presence of two different materials and new insights into the hierarchical organization. Bone. 2014;59:93-104.
67. Fox K, Tran PA, Tran N. Recent Advances in Research Applications of Nanophase Hydroxyapatite. ChemPhysChem. 2012;13(10):2495-506.
68. Bodner L, Manor E, Shear M, Van der Waal I. Primary intraosseous squamous cell carcinoma arising in an odontogenic cyst–a clinicopathologic analysis of 116 reported cases. Journal of oral pathology & medicine. 2011;40(10):733-8.